# Highly Photocatalytic ZnO/In 2 O 3 Heteronanostructures Synthesized by a Coprecipitation Method

**ARTICLE** *in* THE JOURNAL OF PHYSICAL CHEMISTRY C · JANUARY 2009

Impact Factor: 4.77 · DOI: 10.1021/jp8107683



**8 AUTHORS**, INCLUDING:

Zeyan Wang
Shandong University
**89** PUBLICATIONS **2,382** CITATIONS
SEE PROFILE

Baibiao Huang
Shandong University
**370** PUBLICATIONS **9,526** CITATIONS
SEE PROFILE

Ying Dai
Shandong University
**322** PUBLICATIONS **8,474** CITATIONS
SEE PROFILE

Peng Wang
Peking Union Medical College Hospital
**89** PUBLICATIONS **3,182** CITATIONS
SEE PROFILE

# Highly Photocatalytic $ZnO/In_2O_3$ Heteronanostructures Synthesized by a Coprecipitation Method

**Zeyan Wang,[†] Baibiao Huang,*[,†] Ying Dai,[‡] Xiaoyan Qin,[†] Xiaoyang Zhang,[†] Peng Wang,[†] Haixia Liu,[†] and Jiaoxian Yu[†]**

*State Key Laboratory of Crystal Materials, and School of Physics, Shandong University, Jinan 250100, People's Republic of China*

*Received: December 8, 2008; Revised Manuscript Received: January 15, 2009*

We synthesized $ZnO/In_2O_3$ heteronanostructures by a coprecipitation method. Various characterization methods were employed to investigate the structures, morphologies, and photocatalytic properties. The roles of compositions and annealing temperatures on the photocatalytic activities have been systematically studied. The highest photocatalytic efficiency was observed when annealing at 800 °C with the Zn/In ratios of 1:1 in the starting materials. The charge separation process of these heterostructures was also discussed. And the effective separation of the photogenerated electrons and holes was regarded as the main reason for the high photocatalytic activity.

## Introduction

With the development of industry and economy of human society, environmental problems are becoming more and more serious. Since Fujishima and Honda reported the evolution of oxygen and hydrogen from a $TiO_2$ electrode under the irradiation of light in 1972,[1] photocatalysis was regarded as one of the most effective and economical ways to solve the environmental problems. And now it has become a hot spot in scientific research all over the world. Various photocatalysts have been synthesized and studied, such as $TiO_2$, ZnO, $KNbO_3$, $Bi_4Ti_3O_{12}$, etc.[2−8] However, the rapid recombination of photogenerated charge carriers for single semiconductors seriously impeded the improvement of photocatalytic efficiency. Heteronanostructures and p−n junctures by coupling composite semiconductors together would be a beneficial solution for this drawback. Furthermore, it also provides a way to develop efficient photocatalysts from composite semiconductors with proper choice of band gaps and band gap edges to meet the requirements for practical applications. Several systems have been reported, e.g., $TiO_2/SnO_2$, $Co_3O_4/BiVO_4$, $AgCl/H_2WO_4 \cdot H_2O$, etc.,[9−13] and proven to be efficient in photocatalysis.

ZnO with a direct band gap of 3.2 eV is one of the most attractive semiconductor photocatalysts due to its high photosensitivity and stability.[14−16] It is even more efficient than $TiO_2$, the most intensively studied photocatalyst, in the photodegradation of some organic compounds (e.g., acid brown 14).[17] However, the quick recombination of charge carriers is the major limitation in achieving high photocatalytic efficiency. $In_2O_3$ is an indirect band semiconductor with a direct band gap of 3.6 eV and an indirect band gap of 2.8 eV.[18] It was known as an important transparent conducting oxide material and has been widely applied in solar cells, sensor modules, and transparent electrode materials for both electrochromic cells and for liquid crystal display devices.[19,20] $ZnO/In_2O_3$ heterostructure thin film had already been fabricated by various means[21−23] and was applied to flat-panel displays, light-emitting diodes, and thin-film transistors, etc.[24−26] However, the photocatalytic properties of $ZnO/In_2O_3$ heteronanostructure have never been reported. Considering the band edge of ZnO and $In_2O_3$, an efficient heterostructure can be formed for the separation of photogenerated charge carriers, when coupling them together. Furthermore, p−n junctures could also be formed at the interface due to the mutual diffusion of $Zn^{2+}$ and $In^{3+}$ ions,[27,28] which would forward the charge carriers' separation. So we have full reason to believe that $ZnO/In_2O_3$ heterostructures could be a potential candidate for photocatalysis.

Herein, we reported the synthesis of $ZnO/In_2O_3$ heteronanostructures with high photocatalytic activities. A chemical coprecipitation method was employed in our experiments, which is a simple way that can provide both perfect crystalline quality and large surface areas. The roles of composition and annealing temperature on the photocatalytic activities were systematically studied. The optimized composition and annealing temperature has been obtained. And the origin of the high photocatalytic activity for the heterostructure was also discussed.

## Experimental Details

$ZnO/In_2O_3$ heteronanostructures were synthesized by a coprecipitation method in our experiments. Zinc nitrate ($Zn(NO_3)_2 \cdot 6H_2O$), indium nitrate ($In(NO_3)_3 \cdot 4.5H_2O$), and aqueous ammonia of AR grade were employed as starting materials. First, $Zn(NO_3)_2 \cdot 6H_2O$ and $In(NO_3)_3 \cdot 4.5H_2O$ were dissolved into deionized water in a molar ratio of 1:2 to form a clear solution with a $[Zn^{2+}] = 20$ mmol/L. Then, aqueous ammonia was added with constant stirring to the above solution until pH > 9 to ensure complete precipitation. The gel solution was aged for 24 h before filtration. The precipitates were washed by deionized water for several times and dried in an oven at 100 °C. Finally, the samples were obtained after annealing under certain temperatures. In our experiments, five different annealing temperatures were adopted: 600, 700, 800, 900, and 1000 °C, respectively. Samples with different Zn/In ratios (varying from 0.2 to 5) in the starting materials are prepared under identical conditions, in order to investigate the role of composition on the photo-

* Corresponding author. Tel.: +86-531-8836-6324. Fax: +86-531-8836-5969. E-mail: bbhuang@sdu.edu.cn.
[†] State Key Laboratory of Crystal Materials.
[‡] School of Physics.

10.1021/jp8107683 CCC: $40.75 
Published on Web 02/25/2009

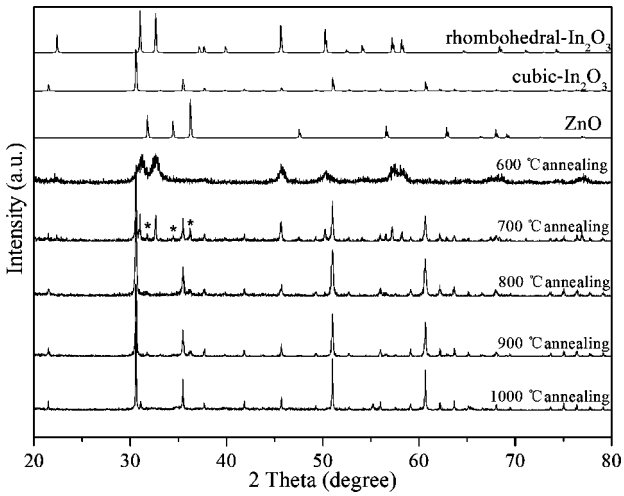


**Figure 1.** XRD patterns of the samples annealed at 600, 700, 800, 900, and 1000 °C.

catalytic activities. For comparison, pure ZnO and $In_2O_3$ nanoparticles are also prepared.

Various characterizations have been employed to test the structures and morphologies of our samples including X-ray diffraction (XRD, Bruker AXS D8 advance powder diffractometer with a Cu Kα X-ray tube), scanning electron microscopy (SEM, Hitachi s-4800), high-resolution transmission electron microscopy (HR-TEM, JEOL JEM-2100; 200 kV). The Brunauer−Emmett−Teller (BET) surface areas were measured with a Builder 4200 instrument at liquid nitrogen temperature. Energy-dispersive spectroscopy (EDS) was employed to determine the actual Zn/In ratios in the products. And the diffuse reflectance spectra were measured on a Shimadzu UV 2550 UV−vis spectrophotometer equipped with an integrating sphere in the wavelength range of 200−800 nm.

Photocatalytic properties were evaluated by the bleaching of methylene blue (MB) dye solvated in water, which is recognized as one of the most standard methods for the evaluation of photooxidation activity. In a typical bleaching test of MB, 50 mg of as-synthesized powder was suspended in 100 mL of MB aqueous solution (pH ∼ 6) with the initial concentration of 20 mg $L^{-1}$ in a glass reactor with a 30 $cm^2$ cross section and 5 cm height. The reactor was then kept in the dark with agitation for 30 min to obtain an adsorption equilibrium, prior to light irradiation by a 300 W Xe arc lamp (PLS-SXE300, Beijing Trusttech Co. Ltd). The efficiency of the degradation processes was evaluated by monitoring the dye decolorization at the maximum absorption around $\lambda = 663$ nm as a function of irradiation time in the separated MB solution with a UV−vis spectrophotometer (Shimadzu UV 2550).

## Results and Discussion

Figure 1 shows the XRD pattern of the samples annealed at different temperatures. We can clearly see that the sample annealed at 600 °C shows a pure phase of rhombohedral $In_2O_3$ without any other compositions. This is mainly because of the poor crystallization of the as-grown sample under the low annealing temperature. When the temperature was increased to 700 °C, a phase transition appeared. The sample showed a mixed phase of rhombohedral and cubic $In_2O_3$ together with a trace of wurtzite ZnO marked with asterisks (*) in Figure 1. When the annealing temperature was higher than 700 °C, the rhombohedral $In_2O_3$ completely disappeared and the samples showed a mixed phase of cubic $In_2O_3$ and wurtzite ZnO. Though the XRD patterns are rather complicated and several phases can be detected in the samples annealed under different temperatures, all the peaks can be fine identified. And no peak shifts or any trace of mixed metal compounds with Zn, In, and O (e.g., $Zn_2In_2O_5$, $Zn_3In_2O_6$, $Zn_4In_2O_7$, etc.) can be detected. Therefore, our samples are considered to be mainly composed by ZnO and $In_2O_3$ with separate phases. The peaks became sharper (the peak width at half-height decreased) and the peak heights of ZnO decreased a little as the annealing temperature increased. That meant the crystallinity of our samples was improved, and the crystal grains grew bigger when the annealing temperature increased, and parts of ZnO may evaporate away at higher temperature. And it is proven by the SEM images and EDS analysis below.

In general, our samples showed a porous structure agglomerated with very small particles and the particle sizes increased with the annealing temperatures. The particle size for the sample annealed under 600 °C is about 10−20 nm with a pore size of about 20 nm (Figure 2a). As the temperature increased, the particle grew bigger and bigger. The mean sizes for the sample annealed at 700, 800, 900, and 1000 °C are 30−40, 40−60, 50−80, and 100−250 nm (Figure 2b−e), respectively. Furthermore, the particles agglomerated more tightly and the pore sizes decreased accordingly. When the annealing temperature is as high as 1000 °C, the pores disappear and the porous structure was completely destroyed as shown in Figure 2e. This observation was further verified by the measurements of the BET surface areas.

The samples annealed under different temperatures varied a lot on the surface areas, and their BET values are listed in Table 1. As we can see in this table, the surface areas of our samples decreased when the annealing temperature increased. The sample annealed at 600 °C showed the highest BET areas of 57.61 $m^2/g$. And the value for the samples annealed at 700 and 800 °C became smaller (15.64 and 12.96 $m^2/g$, respectively). When our samples were annealed at 900 and 1000 °C, the BET surface areas were even smaller (e.g., 2.94 and 0.43 $m^2/g$), only about $^1/_{100}$ the value of the sample annealed at 600 °C. This shows accordance with the morphologies observed by SEM.

The actual Zn/In ratios in our as-synthesized samples were determined by EDS, and the results are shown in Table 1. As we can see, the actual Zn/In ratio in the products decreased constantly as the annealing temperature increased. The actual Zn/In ratio for the sample annealed at 600 °C is 1:2.14, which is close to the starting Zn/In ratio of 1:2. The value decreased to 1:2.5 and 1:2.8 when annealed at 700 and 800 °C, respectively. And small parts of the ZnO may evaporate away. When the annealing temperature is higher (900 and 1000 °C), the actual Zn/In ratio decreased sharply to 1:5.78 and 1:5.81, respectively. More ZnO may evaporate away. This is consistent with the XRD analysis above.

The photocatalytic activities of the $ZnO/In_2O_3$ heteronanostructures were evaluated by the bleaching of MB dye under the irradiation of a Xe arc lamp. As we can see in Figure 3, the photocatalytic activities varied a lot for the samples annealed under different temperatures. The sample annealed at 800 °C showed the highest photocatalytic activity, and more than 97% of MB molecules were decomposed in 120 min, while with the other samples annealed at 600, 700, 900, and 1000 °C, the fractions of the MB dye decomposed in 180 min are estimated to be 37%, 38%, 61%, and 28%, respectively. The huge difference on photocatalytic activities may mainly be due to the effective interfaces exposed to the surface by the two components, where the photocatalytic reactions mainly hap-

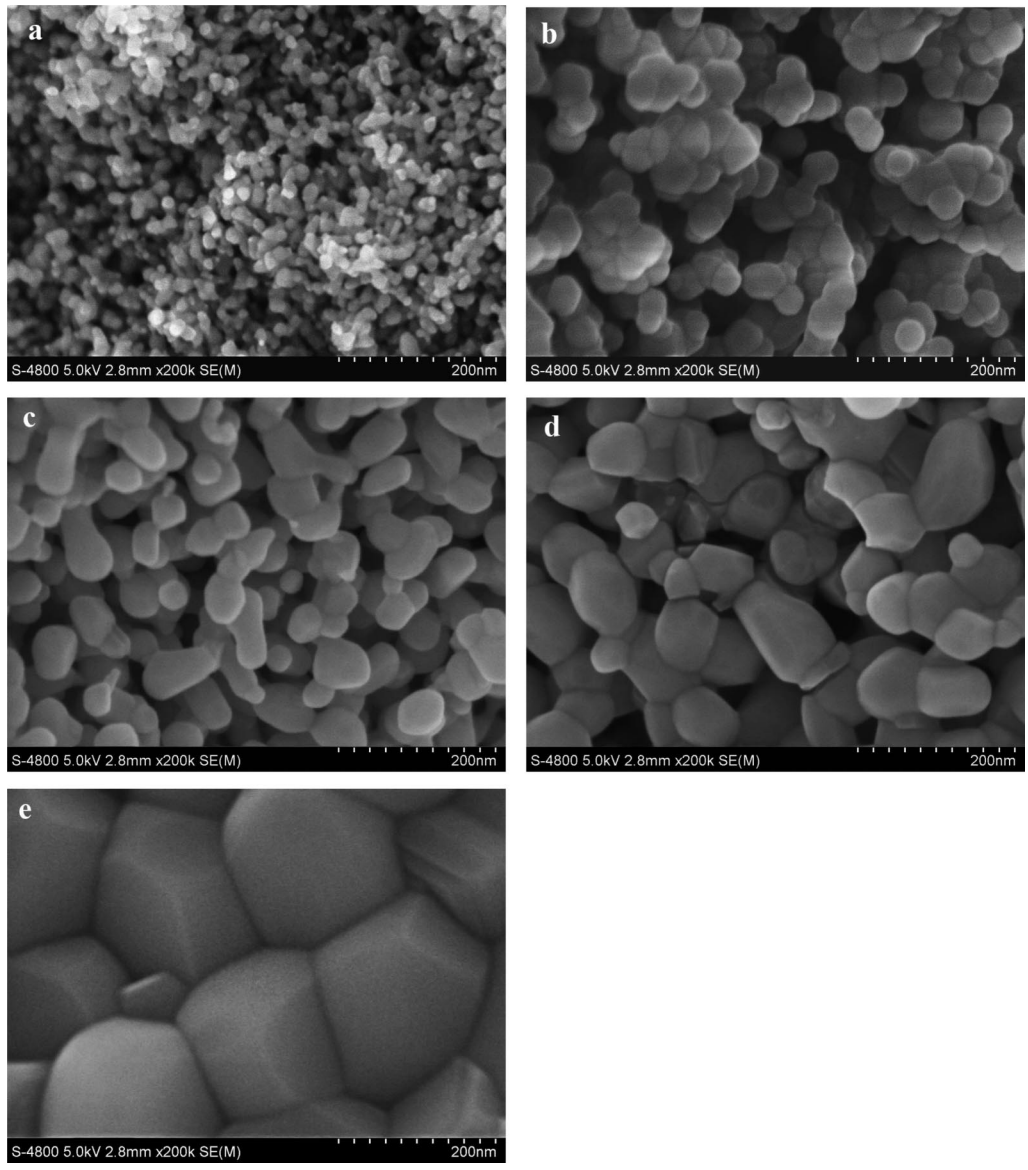


**Figure 2.** SEM images of the samples annealed at (a) 600, (b) 700, (c) 800, (d) 900, and (e) 1000 °C.

**TABLE 1: BET Surface Areas of As-Grown Samples**

| sample | a | b | c | d | e |
|---|---|---|---|---|---|
| annealing temperature | 600 °C | 700 °C | 800 °C | 1: 5.78 | 1000 °C |
| starting Zn/In ratio | 1:2 | 1:2 | 1:2 | 1:2 | 1:2 |
| actual Zn/In ratio | 1:2.14 | 1:2.5 | 1:2.8 | 1:5.78 | 1:5.81 |
| BET area ($m^2$/g) | 57.61 | 15.64 | 12.96 | 2.94 | 0.43 |

pened, and the crystalline qualities of the nanocompositions. Though the samples annealed under 600 and 700 °C show a higher BET surface areas than the sample annealed under 800 °C, the poor crystallinity and the existence of rhombohedral $In_2O_3$ phase maybe the reason for the low photocatalytic activity, whereas the sample annealed at 900 or 1000 °C with better crystalline quality shows smaller BET surface areas and results in poor photocatalytic activities. On the basis of the above analysis, 800 °C was regarded as the optimized annealing temperature in our experiments.

According to Cao, et al.'s report,[29] both of the components of the heterostructures may play an important role on the photocatalytic reactions. So it is important to investigate the samples with different Zn/In ratios in the starting materials. Four more samples with different Zn/In ratios in the starting materials, e.g., 5:1, 2:1, 1:1, and 1:5, respectively, were synthesized under

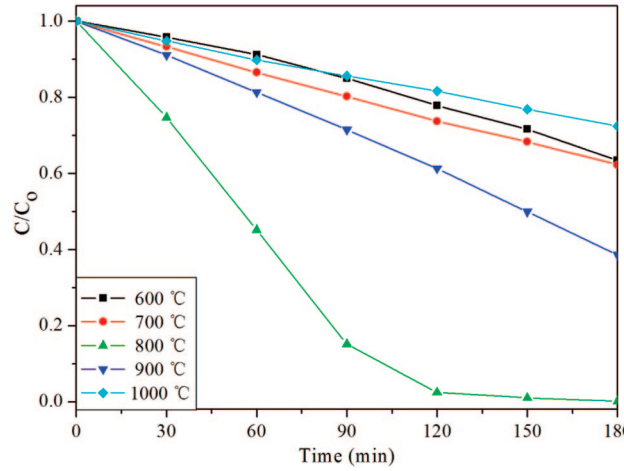


**Figure 3.** Concentration changes of MB dye as a function of irradiation time with the samples annealed under different temperatures.

the optimized annealing temperature of 800 °C. Figure 4a presents the XRD patterns of as-grown samples. As shown in this figure, a mixed phase of cubic $In_2O_3$ and wurtzite ZnO can be detected from all our five samples regardless of the different

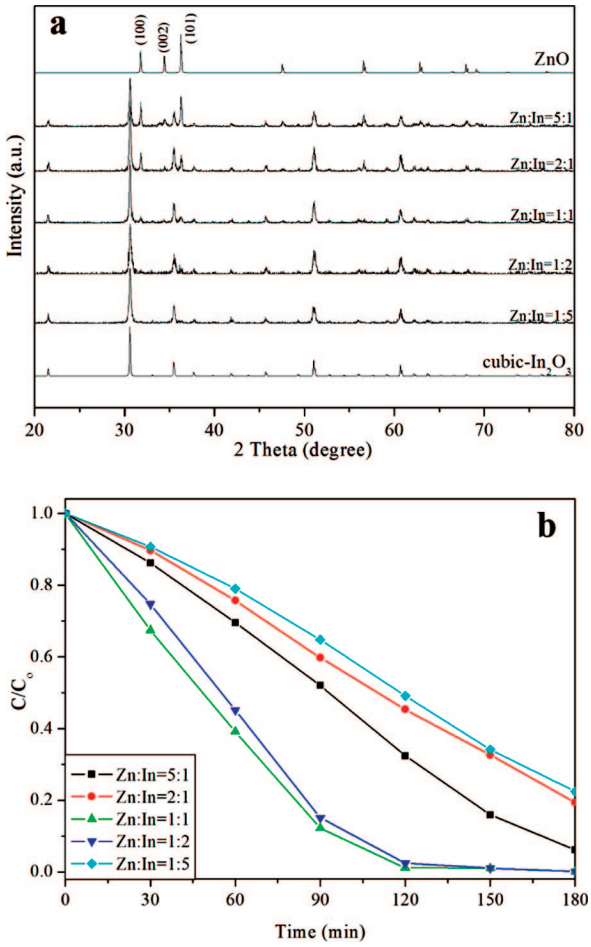


**Figure 4.** (a) XRD patterns and (b) concentration changes of MB dye as a function of irradiation time with the samples with different Zn/In ratios in the starting materials annealed under 800 °C.

Zn/In ratios in the starting materials. The peak heights of the ZnO phase decrease with the Zn/In ratios in the starting mixture and nearly disappear when the Zn/In ratio is 1:5. And it is consistent with the actual Zn/In ratios in the products. The actual Zn/In ratios for the samples with the starting Zn/In ratios of 5:1, 2:1, 1:1, and 1:5 are 1.86:1, 1:1.14, 1:2.24, and 1:5.48, respectively. Figure 4b presents the photocatalytic activities of this group of samples. The samples with the starting Zn/In ratios of 1:1 and 1:2, which have similar Zn/In ratios in the products (1:2.24 vs 1:2.8), showed the highest photocatalytic activities, and more than 97% of MB dye molecular were decomposed in 120 min. The sample with the starting Zn/In ratio of 5:1 shows a next highest photocatalytic activity; about 93% MB molecular were decomposed in 180 min. And the samples with the starting Zn/In ratios of 2:1 and 1:5 show the lowest, and only 67.4% and 65.9% MB were decomposed, respectively.

For comparison, pure $In_2O_3$ and ZnO samples are also prepared under identical conditions. The SEM images and the photocatalytic performance are shown in Figure 5a−c. Both $In_2O_3$ and ZnO show a porous nanostructure agglomerated by small particles which were familiar with the $ZnO/In_2O_3$ bicomponents. And the particle size of $In_2O_3$ is about 20−30 nm and is 200−300 nm for ZnO. In Figure 5c, we can easily find out that the $ZnO/In_2O_3$ heteronanostructures (with a starting Zn/In ratio of 1:1) show a much higher photocatalytic activity than both $In_2O_3$ and ZnO. Only 19.2% of MB molecular for $In_2O_3$ and 67.3% for ZnO were decomposed in 180 min.

In order to investigate the interface of the $ZnO/In_2O_3$ composite, the sample with the starting Zn/In ratio of 1:1 was

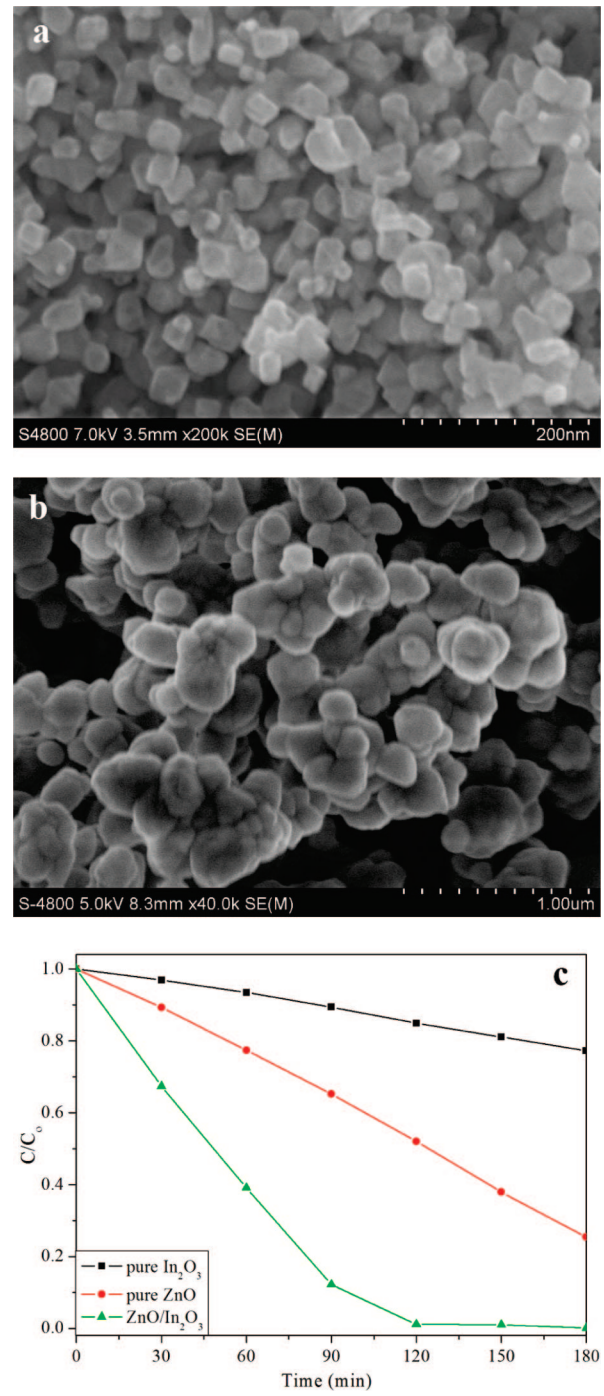


**Figure 5.** SEM images of pure (a) $In_2O_3$ and (b) ZnO synthesized by coprecipitation method and (c) concentration changes of MB dye as a function of irradiation time compared with the $ZnO/In_2O_3$ bicomponents with Zn/In ratio of 1:1 annealed under 800 °C.

chosen to take TEM and HR-TEM characterization. Figure 6a gives an overview of the typical TEM image of the as-synthesized $ZnO/In_2O_3$ composite. Particles with mean sizes of about 40−60 nm can be observed. The atomic resolution HR-TEM image of the magnified view of the black-square area in Figure 6a is shown in Figure 6b. A clear and sharp interface can be seen in this figure. The upper section depicts the lattice-resolved (001) crystalline plane of ZnO with a spacing of 0.281 nm along the [100] direction. The absence of the (002) peak in the XRD patterns shows accordance with the HR-TEM image and indicates the facet structure of ZnO in our experiments. The lower part clearly exhibits the $In_2O_3$ (110) facets with a

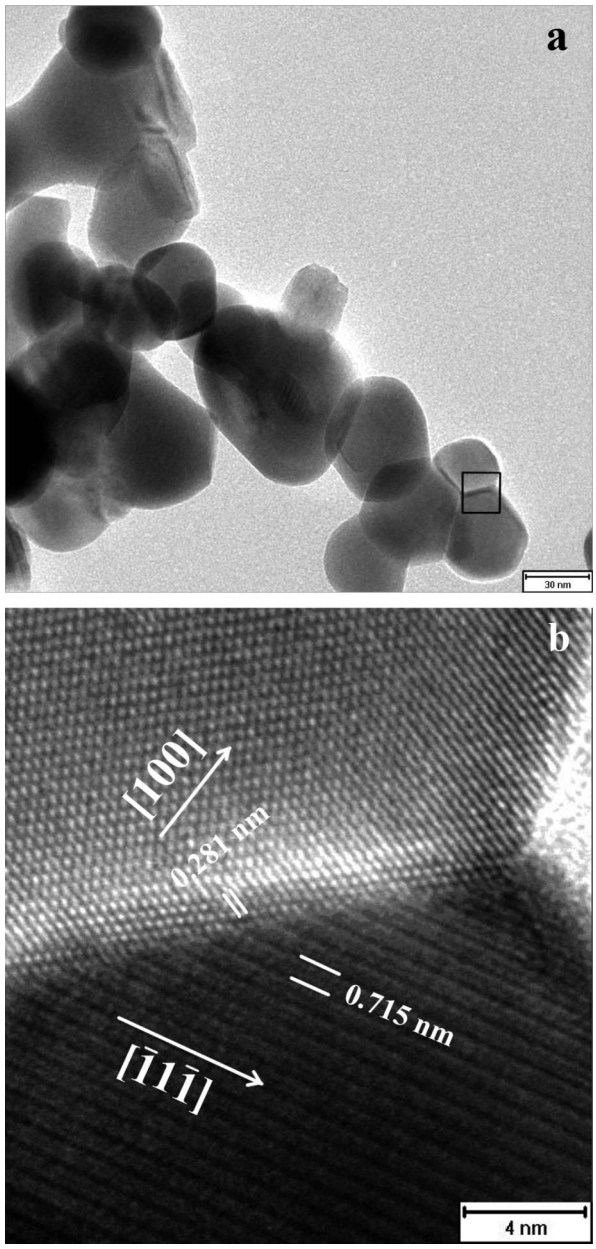


**Figure 6.** (a) TEM image of the $ZnO/In_2O_3$ composites from the sample with the Zn/In ratio of 1:1 in the starting materials annealed under 800 °C; (b) HR-TEM image of the magnified view of the interface between ZnO and $In_2O_3$ shown in the black-square area in panel a.

spacing value of 0.715 nm, which is consistent with the reported value.[30] The good crystalline quality and the sharp interface between ZnO and $In_2O_3$ are advantageous for the separation of the photogenerated charge carriers.

The diffuse reflectance spectrum for the synthesized $ZnO/In_2O_3$ heterostructure is presented in Figure 7. For comparison, the spectra of pure ZnO and $In_2O_3$ synthesized under identical conditions are also plotted. As we can see in this figure, the pure ZnO and $In_2O_3$ show a clear absorption edge at 380 and 480 nm, respectively, whereas the $ZnO/In_2O_3$ composite exhibits a mixed absorption property of both ZnO and $In_2O_3$.

The band energy levels and charge-transfer procedure of ZnO and $In_2O_3$ are shown in Figure 8 schematically. The conduction band (CB) bottom and the valence band (VB) top of ZnO lie at −4.19 and −7.39 eV with respect to absolute vacuum scale (AVS), and the CB bottom and VB top of $In_2O_3$ lie at −3.88 and −6.68 eV versus AVS. Both the CB bottom and the VB

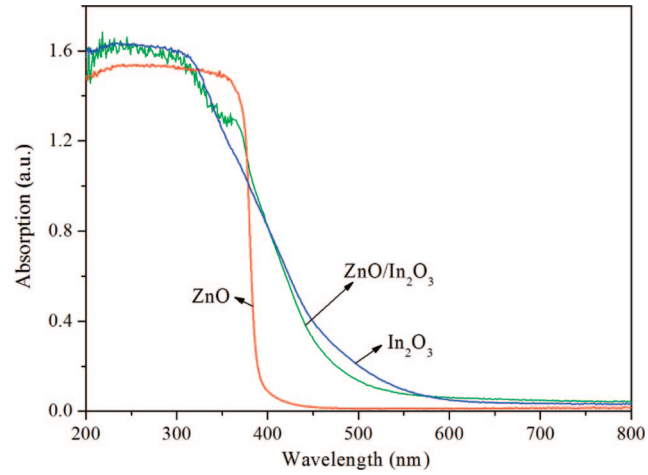


**Figure 7.** Diffuse reflectance spectra of pure ZnO, pure $In_2O_3$, and $ZnO/In_2O_3$ heterostructure.

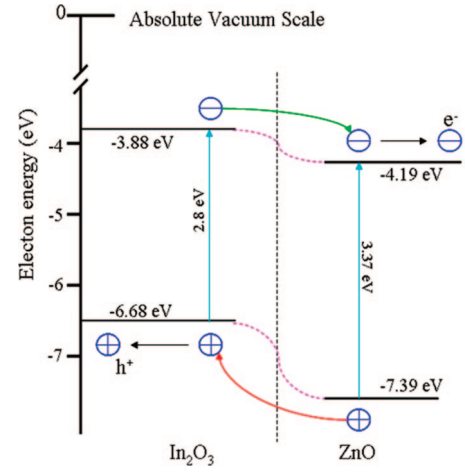


**Figure 8.** Schematic diagram of the band energy levels of ZnO and $In_2O_3$ and the transfer procedure of photogenerated electrons and holes.

top of ZnO lay below the CB bottom and VB top of $In_2O_3$, respectively (Figure 8). When they are coupled together to form a heterostructure, photons may be absorbed in both $In_2O_3$ and ZnO forming electrons and holes. However, an electron at the CB bottom of $In_2O_3$ would migrate to that of the ZnO, whereas a hole at the VB top of $In_2O_3$ would remain there. In contrast, a hole at the VB top of the ZnO would migrate to that of $In_2O_3$, but an electron at the CB bottom of ZnO would remain there, which is energetically favorable. In this way, photogenerated electrons and holes can be efficiently separated. Furthermore, a p−n juncture could be formed at the interface between ZnO and $In_2O_3$. $Zn^{2+}$ and $In^{3+}$ ions could be diffused into the $In_2O_3$ and ZnO lattice, respectively, during the synthetic procedure and cause a doping at the thin layers of the interface. As $Zn^{2+}$-doped $In_2O_3$ exhibited p-type conduction and $In^{3+}$ doping enhanced the n-type conduction of ZnO,[27,28] a p−n juncture could be finally formed at the interface. Therefore, the separation of the photogenerated charge carriers can be further enhanced. The efficient separation of the photogenerated charge carriers is regarded as the key factor for the high photocatalytic activities for the $ZnO/In_2O_3$ system.

Additionally, according to Hoffmann, et al.'s work,[31] during the process of photocatalytic reactions, the photogenerated holes are considered to directly oxidize organic pollutants, whereas the photogenerated electrons are shown to be capable of contributing to the oxidation process through the reduction of

adsorbed $O_2$ to the superoxide radical ion, $^{\bullet}O_2^-$, which can take part in the oxidation process. Therefore, the oxidation of $ZnO/In_2O_3$ could be further improved and result in a high photocatalytic activity.

## Conclusions

We have synthesized $ZnO/In_2O_3$ heteronanostructures by a coprecipitation method. Porous $ZnO/In_2O_3$ nanostructures with heterojunctions have been obtained. The optimized composition and annealing temperatures are obtained by the systematical investigation of the photocatalytic activities of the series of samples with different Zn/In ratios in the starting materials and annealing in different temperatures. And the interface and the energy band structure of the $ZnO/In_2O_3$ composite were also investigated. The $ZnO/In_2O_3$ heteronanostructures are proven to be efficient in the separation of the photogenerated holes and electrons and have a high photocatalytic activities based on our systematic analysis. And the designing of the semiconductor heteronanostructures is regarded as a potential way in the development of future photocatalysts.

**Acknowledgment.** This work was financially supported by a research Grant from the National Basic Research Program of China (No. 2007CB613302) and the National Natural Science Foundation of China (Nos. 50721002 and 10774091).

## References and Notes

(1) Fujishima, A.; Honda, K. *Nature* **1972**, *238*, 37.
(2) Bernhard, K.; Allen, J. B. *J. Am. Chem. Soc.* **1978**, *19*, 100.
(3) Wang, Y.; Li, X.; Lu, G.; Quan, X.; Chen, G. *J. Phys. Chem. C* **2008**, *112*, 7332.
(4) Ding, Q. P.; Yuan, Y. P.; Xiong, X.; Li, R. P.; Huang, H. B.; Li, Z. S.; Yu, T.; Zou, Z. G.; Yang, S. G. *J. Phys. Chem. C* **2008**, *112*, 18846.
(5) Burda, C.; Lou, Y. B.; Chen, X. B.; Samia, A. C. S.; Stout, J.; Gole, J. L. *Nano Lett.* **2003**, *3*, 1049.
(6) Yao, W. F.; Xu, X. H.; Wang, H.; Zhou, J. T.; Yang, X. N.; Zhang, Y.; Shang, S. X.; Huang, B. B. *Appl. Catal., B* **2004**, *52*, 109.
(7) Yao, W. F.; Xu, X. H.; Zhou, J. T.; Yang, X. N.; Zhang, Y.; Shang, S. X.; Wang, H.; Huang, B. B. *J. Mol. Catal. A: Chem.* **2004**, *212*, 323.
(8) Yang, K. S.; Dai, Y.; Huang, B. B.; Whangbo, M.-H. *Chem. Mater.* **2008**, *20*, 6528.
(9) Levy, B.; Liu, W.; Gilbert, S. *J. Phys. Chem. B* **1997**, *101*, 1810.
(10) Liu, Z.; Sun, D. D.; Guo, P.; Leckie, J. O. *Nano Lett.* **2007**, *7*, 1081.
(11) Vinodgopal, K.; Kamat, P. V. *Environ. Sci. Technol.* **1995**, *29*, 841.
(12) Long, M. C.; Cai, W. M.; Cai, J.; Zhou, B. X.; Chai, X. Y.; Wu, Y. H. *J. Phys. Chem. B* **2006**, *110*, 20211.
(13) Wang, P.; Huang, B. B.; Zhang, X. Y.; Qin, X. Y.; Dai, Y.; Jin, H.; Wei, J. Y.; Whangbo, M.-H. *Chem. Eur. J.* **2008**, *14*, 10543.
(14) Carraway, E. R.; Hoffman, A. J.; Hoffmann, M. R. *Environ. Sci. Technol.* **1994**, *28*, 778.
(15) Jang, E. S.; Won, J. H.; Hwang, S. J.; Choy, J. H. *Adv. Mater.* **2006**, *18*, 3309.
(16) Kuo, T. J.; Lin, C. N.; Kuo, C. L.; Huang, M. H. *Chem. Mater.* **2007**, *19*, 5143.
(17) Sakthivel, S.; Neppolian, B.; Shankar, M. V.; Arabindoo, B.; Palanichamy, M.; Murugesan, V. *Sol. Energy Mater. Sol. Cells* **2003**, *77*, 65.
(18) Quarto, F.; Sunseri, C.; Piazza, S.; Romano, M. *J. Phys. Chem. B* **1997**, *101*, 2519.
(19) Hamburg, I.; Granqvist, C. G. *J. Appl. Phys.* **1986**, *60*, 123.
(20) Li, X.; Wanlass, M. W.; Gessert, T. A.; Emery, K. A.; Coutts, T. J. *Appl. Phys. Lett.* **1989**, *54*, 2674.
(21) Ku, D. Y.; Kim, I. H.; Lee, I.; Lee, K. S.; Lee, T. S.; Jeong, J.-H.; Baik, Y.-J.; Kim, W. M. *Thin Solid Films* **2006**, *515*, 1364.
(22) Lo, C. Y.; Hsu, C. L.; Yu, Q. X.; Lee, H. Y.; Lee, C. T. *J. Appl. Phys.* **2002**, *92*, 274.
(23) Lee, J.-H.; Lee, S.-Y.; Park, B.-O. *Mater. Sci. Eng., B* **2006**, *127*, 267.
(24) Song, Y. S.; Park, J. K.; Kim, T. W.; Chung, C. W. *Thin Solid Films,* **2004**, *467*, 117.
(25) Kim, H.-K. *Surf. Coat. Technol.* **2008**, *203*, 652.
(26) Yaglioglu, B.; Yeom, H. Y.; Beresford, R.; Paine, D. C. *Appl. Phys. Lett.* **2006**, *89*, 062103.
(27) Huang, Y. H.; Zhang, Y.; Gu, Y. S.; Bai, X. D.; Qi, J. J.; Liao, Q. L.; Liu, J. *J. Phys. Chem. C* **2007**, *111*, 9039.
(28) Mohammad-Mehdi, B. M.; Mehrdad, S. S. *Semicond. Sci. Technol.* **2003**, *18*, 97.
(29) Cao, Y.; Zhang, X.; Yang, W.; Hui, D.; Bai, Y.; Li, T.; Yao, J. *Chem. Mater.* **2000**, *12*, 3445.
(30) Dai, L.; Chen, X. L.; Jian, J. K.; He, M.; Zhou, T.; Hu, B. Q. *Appl. Phys. A: Mater. Sci. Process.* **2002**, *75*, 187.
(31) Hoffmann, M. R.; Martin, S. T.; Choi, W.; Bahnemann, D. W. *Chem. Rev.* **1995**, *95*, 69.

JP8107683